Optics Letters

CEP-stable few-cycle pulses with more than 190 μJ of energy at 100 kHz from a noncollinear optical parametric amplifier

Federico J. Furch,[1,*] Tobias Witting,[1] Achut Giree,[1] Chao Luan,[1] Felix Schell,[1] Gunnar Arisholm,[2] Claus P. Schulz,[1] and Marc J. J. Vrakking[1]

[1]Max Born Institute for Nonlinear Optics and Short Pulse Spectroscopy, Max-Born-Straße 2a, 12489 Berlin, Germany
[2]Norwegian Defence Research Establishment (FFI), P.O. Box 25, 2027 Kjeller, Norway
*Corresponding author: furch@mbi-berlin.de

Received 5 May 2017; accepted 29 May 2017; posted 2 June 2017 (Doc. ID 295320); published 22 June 2017

Noncollinear optical parametric amplifiers (NOPAs) have become the leading technique for the amplification of carrier-envelope phase (CEP)-stable, few-cycle pulses at high repetition rate and high average power. In this Letter, a NOPA operating at a repetition rate of 100 kHz delivering more than 24 W of average power before compression is reported. The amplified bandwidth supports sub-7 fs pulse durations and pulse compression close to the transform limit is realized. CEP stability after amplification is demonstrated. The system paves the way to attosecond pump-probe spectroscopy with electron–ion coincidence detection.

OCIS codes: (320.0320) Ultrafast optics; (320.7110) Ultrafast nonlinear optics; (190.4970) Parametric oscillators and amplifiers; (320.7160) Ultrafast technology.

https://doi.org/10.1364/OL.42.002495

In the past decade, the availability of coherent light pulses in the extreme ultraviolet (XUV) with sub-femtosecond pulse durations has enabled the emergence of the field of attosecond science [1]. Isolated attosecond pulses (IAPs) in the XUV are typically produced through high-order harmonic generation (HHG) driven with intense, carrier-envelope phase (CEP)-stable, few-cycle laser pulses operating at optical frequencies, in combination with a gating technique that confines the XUV emission to a single half-cycle of the driver laser pulses [2–4].

Energetic, CEP-stable laser pulses in the near infrared (NIR) with pulse durations down to a few femtoseconds (i.e., only a few optical cycles) are nowadays routinely generated in many laboratories around the world. Most systems rely on the combination of Ti:sapphire laser amplifiers and pulse post-compression in a gas-filled, hollow-core fiber [5]. These systems can generate few-cycle pulses with energies ranging from hundreds of μJ to a few mJ at a few kHz repetition rate and have been successfully implemented in experimental setups in which the few-cycle pulses are combined with IAPs in a pump-probe configuration, to study ultrafast electronic processes in atoms, molecules, and solids [1]. Typically, the observables in these experiments are the velocity distributions of ions and electrons, or the transient absorption spectrum of the XUV pulse. In the former case, a more attractive technique to analyze the complex scenarios that arise during the pump-probe experiment is the detection of the momentum vectors of all produced photo-electrons and photo-ions in coincidence, utilizing a reaction microscope [6]. However, coincidence detection demands that at most one ionization event occurs per laser shot, and therefore high-repetition-rate experiments are required. The implementation of attosecond pump-probe experiments with coincidence detection is so far limited by the properties of available Ti:sapphire amplifiers to a maximum repetition rate of 10 kHz [7]. Although this is a remarkable achievement, operation at much higher repetition rates is highly desirable.

Recently, noncollinear optical parametric amplifiers (NOPAs) have become a very attractive tool for amplifying ultrashort laser pulses over a broad spectral range, from the visible to the mid-infrared. The achievable high gains over a broad gain bandwidth, and the highly reduced heat load as compared to traditional laser amplifiers, make NOPAs very well suited for the amplification of few-cycle pulses at high repetition rates. High-repetition-rate (≥100 kHz) NOPAs around 800 nm amplifying few-cycle pulses from Ti:sapphire oscillators have been demonstrated for a wide range of pulse energies, repetition rates, and average powers [8–11]. However, up to now, few-cycle, 100 μJ-level pulses have not yet been achieved at these repetition rates. The combination of high energy and high repetition rate has been reported, so far, only for parametric amplifiers operating in burst-mode and delivering longer pulses [12,13], and for longer pulses from fiber-based laser amplifiers post-compressed in gas-filled, hollow-core waveguides. In the latter case, CEP stability has yet to be demonstrated [14].

In this Letter, a NOPA operating at a central wavelength of approximately 790 nm, delivering more than 24 W of output power, is demonstrated. After compression, a broadband variable power attenuator and parasitic second-harmonic filtering, 7 fs pulses with more than 190 μJ pulse energy at a repetition

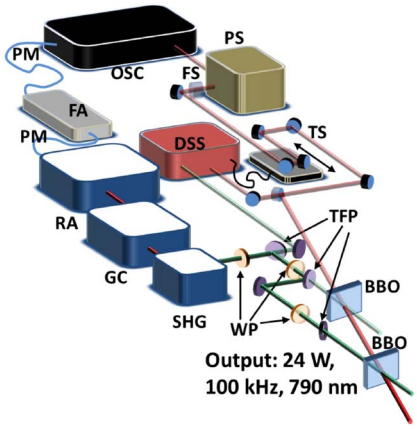

Fig. 1. Block diagram of the noncollinear optical parametric amplification (NOPA) system. OSC, Ti:sapphire laser oscillator; PM, polarization-maintaining fiber; FA, fiber stretcher and fiber amplifiers; RA, regenerative amplifier; GC, grating compressor; SHG, second-harmonic generation module; PS, pulse shaper; FS, fused-silica window for pulse stretching; DSS, delay stabilization system; TS, translation stage; WP, $\lambda/2$ wave plate; TFP, thin-film polarizer; BBO, BBO crystal.

rate of 100 kHz (more than 19 W of average power), are available for experiments.

A block diagram of the system is shown in Fig. 1. An octave-spanning, carrier-envelope offset-frequency (CEO)-stabilized Ti:sapphire oscillator (Venteon Pulse:One) is utilized to seed the NOPA and the pump laser for the NOPA. A fraction of the oscillator (OSC) radiation with approximately 10 nm of bandwidth centered around 1030 nm is filtered out with a dichroic mirror, coupled into a polarization-maintaining optical fiber and used to seed a chirped pulse amplification (CPA) system from Trumpf Scientific. The CPA consists of a fiber Bragg grating stretcher, several Yb-doped fiber pre-amplifiers (FA), a regenerative thin-disk Yb:YAG amplifier (RA), and a grating compressor (GC). After second-harmonic generation (SHG), the pulses from the CPA are used to pump the NOPA. The CPA system delivers up to 120 W at 515 nm, in 900 fs pulses at a repetition rate of 100 kHz. The few-cycle pulses generated in the OSC pass through a commercial pulse shaper (PS) based on a spatial light modulator (SLM) (Biophotonics Solutions Inc., MIIPS Box 640 P). Subsequently, the pulses are split using a beam splitter that sends 3% of the incoming power to a delay stabilization system (DSS), with the rest seeding the NOPA. The DSS consists of a NOPA stage whose amplified spectrum is analyzed for active stabilization of the delay between the pump and seed pulses in the NOPA. The setup is similar to that proposed in Ref. [15], except that all the signal processing is done digitally. When the delay is actively stabilized by means of a delay stage in the seed arm, a residual temporal jitter of 4 fs rms is achieved over a period of several hours.

The seed pulses are amplified in two NOPA stages based on β-Barium Borate (BBO) crystals under type-I phase matching and walk-off compensation (WOC) geometry. The noncollinear and phase-matching angles, the intensity of the pump in each crystal, and the power splitting between the stages were designed with the support of numerical simulations carried out with the code Sisyfos (SImulation SYstem For Optical Science) [16]. A $\lambda/2$ wave plate and a thin-film polarizer are employed to divide the pump power between the first and second amplification stages. The first stage is pumped by 120 μJ pulses (12 W) at an intensity of 100 GW/cm^2. Pulses with energies up to 960 μJ (96 W) are utilized to pump the second stage, with the pump intensity 50 GW/cm^2.

A flat phase was introduced at first in the SLM of the PS. However, the optical arrangement of the PS introduces a non-negligible amount of dispersion. This, in combination with a few meters of propagation in air and a 5-mm-thick fused silica window is utilized to stretch the seed pulses to approximately 300 fs. In the first stage, the seed pulses are amplified from 250 pJ to 12 μJ (1.2 W of average output power) in a 2.5-mm-thick BBO crystal. This means the amplification stage has a high gain of approximately 48,000 and a moderate pump-to-signal energy conversion efficiency of 10%. In the second stage, the pulses are amplified in a 3-mm-thick BBO crystal from 12 μJ to a maximum pulse energy of 242 μJ (24.2 W of average power, mean value over 2.5 h) when the pump power is 96 W and the pump peak intensity slightly over 50 GW/cm^2. This stage has a gain of 20.2 and a high conversion efficiency of 24%.

In both NOPA stages, the noncollinear angle was set to the so-called "magic angle," i.e., the angle where the projection of the group velocity of the idler onto the direction of the signal beam equals the group velocity of the signal. This configuration not only ensures a broad amplification bandwidth [17] but is also known to minimize angular dispersion of the amplified signal beam [18]. The phase-matching angles and pump-seed delays were adjusted to maximize the output power. The total conversion efficiency of the two-stage amplifier amounts to 22.4%. In Fig. 2, the output power measured over two-and-a-half hours is shown. The output power fluctuations are characterized by a root mean square value of 1%, which is at the same level as the pump laser. The slow drift corresponds to changes in the output power of the pump. Under these same conditions, an upper limit for the content of amplified optical parametric fluorescence was estimated by measuring the output power of the amplifier when the seed was blocked at the entrance to the first stage, while leaving all the delays, angles, and overlaps optimal. The resulting power was 200 mW, less than 1% of the total output power when the amplifier is seeded.

The amplified signal beam (measured after approximately two meters of propagation) has a round shape, and the power is distributed slightly asymmetrically towards one side along the walk-off plane. This beam profile and the far-field beam profile

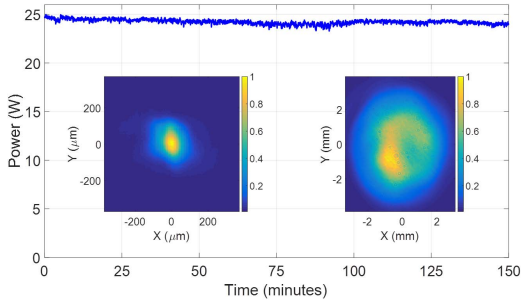

Fig. 2. Output power of the system measured over two-and-a-half hours. The insets show the amplified beam after 2 m of propagation (right) and at the focal plane of a 1-m-focal-length mirror (left).

are shown in the insets in Fig. 2. For the far-field measurement, the beam size was reduced by a factor of two in a telescope and subsequently focused by a 1-m-focal-length spherical mirror. In addition, the beam profile was measured after approximately 4 m of propagation under different pump power levels between 35 W and 96 W, in order to detect any thermal effect at high-average pump power. No appreciable changes were observed in the amplified beam.

The spectrum after the second stage covers the range 670–1025 nm. The transform-limited pulse duration supported by the high-energy pulse spectrum is 6.6 fs. To realize the temporal compression of the amplified pulses, the PS in Fig. 1 was utilized in combination with a set of chirped mirrors (Laser Quantum DCM11) and a pair of thin fused silica wedges, located after the amplification stages (not shown in Fig. 1).

The laser pulses were characterized utilizing a SEA-F-SPIDER device [19]. We made use of the multiple-shearing algorithm [20] to faithfully reconstruct the spectral phase across the dips in our spectrum [21]. In order to avoid damage to the optical components in the SEA-F-SPIDER and reduce the intensity at focus, the power was attenuated by a broadband half-wave plate and thin-film polarizer in combination with a set of chirped mirrors specifically designed to compensate for material dispersion of the wave plate and the polarizer (Spectra-Physics, Femtooptics OA331). The broadband variable power attenuator is important in applications, in order to continuously change the laser power sent towards the experiments.

The compression followed a two-step approach. In the first step, a flat phase was introduced in the SLM of the PS, the amplification conditions were optimized, and the chirped mirrors and the fused silica wedges were utilized to minimize the group delay dispersion (GDD) of the amplified pulses. In addition to the already mentioned optical elements, a dichroic mirror was inserted in the optical path to remove the parasitic second-harmonic radiation produced during amplification, due to the chosen WOC geometry [22]. During the second step of the pulse compression, the third-order and fourth-order dispersion terms of the spectral phase were adjusted in the PS while monitoring the pulse temporal shape in the SEA-F-SPIDER. By introducing only small corrections ($+100$ fs^3, $+600$ fs^4) to the spectral phase in the PS, the compressed pulse duration could be changed without significantly affecting the amplification conditions in the NOPA. The SEA-F-SPIDER measured the spectrum and spectral phase along a spatial dimension of the beam. Here we present results corresponding to measurements along the walk-off plane, where spatio-temporal distortions are more likely to affect the amplified field [23].

For the results in Fig. 3, an integration over the spatial coordinate was performed corresponding to $1/e^2$ of the beam size. In addition, the measurement was repeated 25 times over a time span of 90 s, in order to test the short-term stability of the NOPA output. The colored traces in Figs. 3(a)–3(c) are the results of these 25 different measurements. For all measurements, we used the two shears 10 mrad/fs and 50 mrad/fs. Figure 3(a) shows the measured spectra. The mean center frequency is 2.363 rad/fs (797 nm), with a fluctuation of only 0.002 rad/fs (≡0.08%) over the 25 measurements. This stability is a result of the active pump-seed DSS. In Fig. 3(b), the retrieved spectral phases are presented, and Fig. 3(c) shows the corresponding temporal

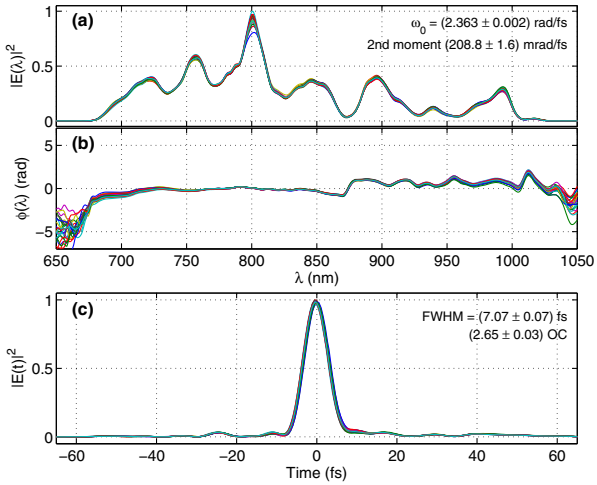

Fig. 3. Pulse characterization. We recorded 25 successive pulse measurements over a time span of 1.5 min. Measured spectra (a), spectral phases (b), and retrieved temporal shapes (c) of the amplified pulses.

intensity envelopes of the complex electric fields. The measured pulse duration was (7.07 ± 0.07) fs full width at half-maximum (FWHM), only a factor 1.07 longer than the transform-limited pulse duration, and corresponding to 2.65 optical cycles. The confidence value provided for the pulse duration represents the standard deviation of the series of 25 measurements. Moreover, the relatively clean pulse compression ensures that only a small fraction of the energy is lost to satellite pulses. More than 82% of the energy is located in the main pulse, while for the transform-limited pulse shape, the fraction of energy in the main pulse reaches 92%. The measured spectral phases consistently show a phase jump around 875 nm where the parasitic second harmonic is phase matched. This also manifests in a dip in the amplified spectrum. As discussed in Ref. [23], the jump in the spectral phase is a natural result of amplification in the WOC geometry. The measurement series was repeated by rotating the beam and measuring perpendicular to the walk-off plane, obtaining similar results. After losses in the chirped mirrors, the broadband variable power attenuator and the filter for the removal of the parasitic second harmonic, the compressed output power exceeds 19 W, i.e., the pulse energy exceeds 190 μJ.

Since the OSC pulses seeding the NOPA are CEO frequency-stabilized, a proper choice of the repetition rate in the CPA system pumping the NOPA ensures that the amplified ultrashort pulses carry the same CEP, as it was already shown in Refs. [8–11] and elsewhere. In the system introduced here, the OSC repetition rate is 80 MHz, and the CEO frequency is stabilized to one-fourth of the repetition rate. Therefore, any repetition rate in the CPA system that is an exact divisor of 20 MHz, as is the case for 100 kHz, ensures that the amplified pulses in the NOPA carry the same CEP. The stability of the CEP after amplification was characterized by measuring spectral interference fringes with a home-built, common-path f-to-2f interferometer, while the NOPA was operating at the maximum output power. The interferometric signal was measured with a commercial spectrometer (HR4000, Ocean Optics) and processed with a portable computer. During all CEP measurements, the acquisition time in the spectrometer was set to the lowest possible value, 1 ms; therefore, all

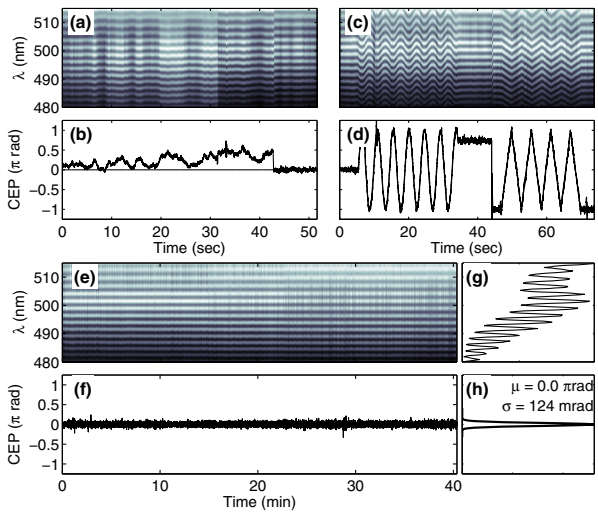

Fig. 4. CEP stability and control of the amplified pulses. (a, c, e) are measured f-to-2f interference fringes as a function of time, and (b, d, f) show the extracted CEP values in units of π rad. In (a) and (b), we show the CEP drift of the amplified pulses with engaged fast loop; from 42 s onwards, both the fast and slow loops are engaged. In (c) and (d), arbitrary control of the CEP with a sine and a triangle modulation is shown. (e) and (f) show long-term CEP measurements over a duration of 40 min. (g) shows the fringe modulation depth. (h) Histogram of the entire dataset.

interferograms average over 100 laser shots. We extract the relative CEP value from the fringe pattern with a fast Fourier transform (FFT)-based algorithm and feed an analog DC voltage to the offset input of the fast-feedback loop electronics of the OSC. The acquisition and slow-feedback loop operated at a speed of 105 Hz, limited by the data transfer rate from the spectrometer. Figure 4 shows the f-to-2f interference fringes and evaluated CEP phases. In Figs. 4(a) and 4(b), the f-to-2f fringes and CEP are shown without slow-loop correction (i.e., only the OSC CEO-locking feedback loop is engaged) for 42 s. The phase of the interference pattern, and therefore the CEP of the amplified pulses, changes slowly over time with an amplitude of $\approx 0.5\pi$ rad and a period on the order of 10 s. Between $t = 20$ s and 31 s, the pump-seed DSS was turned off. As a result, the spectrum of the NOPA changes slightly, changing the white light generation and the contrast of the fringes. Around $t = 42$ s, the slow-CEP-feedback loop is turned on and the phase stays close to 0π rad. Figures 4(c) and 4(d) illustrate arbitrary control of the CEP of the amplified laser pulses. In our feedback software, we set the CEP target to a sine and a triangle wave of 2π amplitude. Figures 4(c) and 4(d) show the f-to-2f interference fringes and extracted CEP phases, respectively. Figures 4(e) and 4(f) show the measured fringes and CEP values over 40 min recorded at 105 Hz acquisition rate. Figure 4(g) shows the modulation depth of the fringe pattern. A histogram of all CEP values over 40 min is shown in Fig. 4(h). The CEP jitter evaluated from all 252,000 datapoints is 124 mrad rms. In future work, the pulse-to-pulse stability of the CEP, crucial for the success of pump-probe experiments with attosecond time resolution, will be evaluated on a single-shot basis at 100 kHz.

In conclusion, a NOPA system delivering more than 24 W of average power at 100 kHz has been demonstrated. After compression using chirped mirrors and thin fused-silica wedges, a broadband variable power attenuator, and removal of parasitic second harmonic, more than 190 μJ of energy are obtained in close-to-transform-limited few-cycle pulses with a duration of 7.07 fs, which represents, to the best of our knowledge, the highest pulse energy reported so far for CEP-stable, few-cycle pulses operating at these high repetition rates. The system will be employed for HHG and isolated attosecond pulse production, and will be the basis of an attosecond pump-probe beamline with coincidence detection capabilities.

Funding. FP7 People: Marie-Curie Actions (PEOPLE) (316687); Horizon 2020 Framework Programme (H2020) (Laserlab-Europe EU-H2020 654148, 674960).

REFERENCES

1. F. Krausz and M. Ivanov, Rev. Mod. Phys. **81**, 163 (2009).
2. M. Hentschel, R. Kienberger, C. Spielmann, G. A. Reider, N. Milosevic, T. Brabec, P. Corkum, U. Heinzmann, M. Drescher, and F. Krausz, Nature **414**, 509 (2001).
3. G. Sansone, E. Benedetti, F. Calegari, C. Vozzi, L. Avaldi, R. Flammini, L. Poletto, P. Villoresi, C. Altucci, R. Velotta, S. Stagira, S. D. Silvestri, and M. Nisoli, Science **314**, 443 (2006).
4. K. T. Kim, C. Zhang, T. Ruchon, J.-F. Hergott, T. Auguste, D. M. Villeneuve, P. B. Corkum, and F. Quéré, Nat. Photonics **7**, 651 (2013).
5. M. Nisoli, S. D. Silvestri, O. Svelto, R. Szipöcs, K. Ferencz, C. Spielmann, S. Sartania, and F. Krausz, Opt. Lett. **22**, 522 (1997).
6. J. Ullrich, R. Moshammer, A. Dorn, R. Dörner, L. P. H. Schmidt, and H. Schmidt-Böcking, Rep. Prog. Phys. **66**, 1463 (2003).
7. M. Sabbar, S. Heuser, R. Boge, M. Lucchini, L. Gallmann, C. Cirelli, and U. Keller, Rev. Sci. Instrum. **85**, 103113 (2014).
8. S. Prinz, M. Haefner, C. Y. Teisset, R. Bessing, K. Michel, Y. Lee, X. T. Geng, S. Kim, D. E. Kim, T. Metzger, and M. Schultze, Opt. Express **23**, 1388 (2015).
9. J. Matyschok, T. Lang, T. Binhammer, O. Prochnow, S. Rausch, M. Schultze, A. Harth, P. Rudawski, C. L. Arnold, A. L'Huillier, and U. Morgner, Opt. Express **21**, 29656 (2013).
10. J. Rothhardt, S. Demmler, S. Hädrich, J. Limpert, and A. Tünnermann, Opt. Express **20**, 10870 (2012).
11. F. J. Furch, A. Giree, F. Morales, A. Anderson, Y. Wang, C. P. Schulz, and M. J. J. Vrakking, Opt. Express **24**, 19293 (2016).
12. H. Höppner, A. Hage, T. Tanikawa, M. Schulz, R. Riedel, U. Teubner, M. J. Prandolini, B. Faatz, and F. Tavella, New J. Phys. **17**, 053020 (2015).
13. M. Pergament, G. Palmer, M. Kellert, K. Kruse, J. Wang, L. Wissmann, U. Wegner, M. Emons, D. Kane, G. Priebe, S. Venkatesan, T. Jezynski, F. Pallas, and M. J. Lederer, Opt. Express **24**, 29349 (2016).
14. S. Hädrich, M. Kienel, M. Müller, A. Klenke, J. Rothhardt, R. Klas, T. Gottschall, T. Eidam, A. Drozdy, P. Jójárt, Z. Várallyay, E. Cormier, K. Osvay, A. Tünnermann, and J. Limpert, Opt. Lett. **41**, 4332 (2016).
15. S. Prinz, M. Häfner, M. Schultze, C. Y. Teisset, R. Bessing, K. Michel, R. Kienberger, and T. Metzger, Opt. Express **22**, 31050 (2014).
16. G. Arisholm, J. Opt. Soc. Am. B **14**, 2543 (1997).
17. G. M. Gale, M. Cavallari, T. J. Driscoll, and F. Hache, Opt. Lett. **20**, 1562 (1995).
18. J. Bromage, C. Dorrer, and J. D. Zuegel, Opt. Lett. **35**, 2251 (2010).
19. T. Witting, F. Frank, C. A. Arrell, W. A. Okell, J. P. Marangos, and J. W. G. Tisch, Opt. Lett. **36**, 1680 (2011).
20. D. R. Austin, T. Witting, and I. A. Walmsley, J. Opt. Soc. Am. B **26**, 1818 (2009).
21. D. R. Austin, T. Witting, and I. A. Walmsley, Opt. Lett. **35**, 1971 (2010).
22. J. Bromage, J. Rothhardt, S. Hädrich, C. Dorrer, C. Jocher, S. Demmler, J. Limpert, A. Tünnermann, and J. D. Zuegel, Opt. Express **19**, 16797 (2011).
23. A. Giree, M. Mero, G. Arisholm, M. J. J. Vrakking, and F. J. Furch, Opt. Express **25**, 3104 (2017).